NANO · MICRO small
www.small-journal.com

# Fano-Like Resonance from Disorder Correlation in Vacancy-Doped Photonic Crystals

*Jose Angel Pariente, Farzaneh Bayat, Alvaro Blanco, Antonio García-Martín, Carlos Pecharromán, Manuel I. Marqués, and Cefe López**

**By preparing colloidal crystals with random missing scatterers, crystals are created where disorder is embodied as vacancies in an otherwise perfect lattice. In this special system, there is a critical defect concentration where light propagation undergoes a transition from an all but perfect reflector (for the spectral range defined by the Bragg condition), to a metamaterial exhibiting an enhanced transmission phenomenon. It is shown that this behavior can be phenomenologically described in terms of Fano-like resonances. The results show that the Fano's parameter *q* experiences a sign change signaling the transition from a perfect crystal exhibiting a reflectance Bragg peak, through a state where background scattering is maximum and Bragg reflectance reaches a minimum to a point where the system reenters a low scattering state recovering ordinary Bragg diffraction. A simple dipolar model considering the correlation between scatterers and vacancies is proposed and the reported evolution of the Fano-like scattering is explained in terms of the emerging covariance between the optical paths and polarizabilities and the effect of field enhancement in photonic crystal (PhC) defects.**

## 1. Introduction

Understanding how the arrangement of defects in photonic crystals (PhC) impacts their photonic properties is crucial for the design of functional materials. Sparse defects can be assumed isolated and are well understood. The opposite, fully disordered scatterers that form photonic glasses, present other kinds of features but are also fairly well understood. There is, however, a middle region where defects can be assumed neither few and isolated nor so abundant that either band theory or single scattering approaches offer ready help.

Resonances are undoubtedly one of the most deeply studied phenomena in the history of physics.[1] From the atomic scale[2] to celestial mechanics,[3] not forgetting the perpetual harmonic oscillator,[4] resonances are present in any type of system due to the simplicity of their description and the processes involved. For wave physics in general and for photonics, in particular, resonances are the cornerstone on which plenty of devices are based. In this sense, they can be the result of the interaction of light with the structure as in waveguides,[5] dielectric nanostructures,[6] and random lasers,[7] or by using resonators that exploit well-known photonic properties such as those based on Fabry–Perot oscillations,[8] Bragg,[9] or Mie scattering.[10]

A singular example of resonance is Fano's resonance. Generally speaking, Fano resonance appears in perturbed systems where two transition channels interfere, one associated to a discrete state (narrow band) and the other to a continuum of states (broadband).[11] The "fingerprint" in this type of resonance is the lineshape asymmetry contained in the Fano *q* parameter, whose value defines the weight of each channel involved in the interference.[12] Additionally, this parameter indicates whether the system presents a high degree of resonance (higher values of *q*) or it is mostly dissipative (close to zero values of *q*). Work in numerous areas succeeded in identifying this type of resonance by their asymmetric peaks.[13] In photonics, in particular, Fano's resonance has gathered a great deal of attention in the last few years[14] as a tool to enhance light emission in metasurfaces,[15] in the development of photonic molecules,[16] or to improve sensitivity of hybrid PhC,[17] and plasmonic sensors[18] among others.[19]

J. A. Pariente, F. Bayat[+], A. Blanco, C. Pecharromán, C. López[++]
Instituto de Ciencia de Materiales de Madrid (ICMM)
Consejo Superior de Investigaciones Científicas (CSIC)
Calle Sor Juana Inés de la Cruz 3, Madrid E-28049, Spain
E-mail: c.lopez@csic.es

A. García-Martín
Instituto de Micro y Nanotecnología (IMN-CNM)
Consejo Superior de Investigaciones Científicas (CSIC)
Isaac Newton 8 (PTM), Tres Cantos, Madrid E-28760, Spain

M. I. Marqués
Departamento de Física de Materiales & Condensed Matter Physics Center (IFIMAC) & Nicolás Cabrera Institute
Universidad Autónoma de Madrid (UAM)
Av. F. Tomás y Valiente, Madrid 28049, Spain

The ORCID identification number(s) for the author(s) of this article can be found under https://doi.org/10.1002/smll.202302355

[+]Present address: Department of Physics, Azarbaijan Shahid Madani University (ASMU), Tabriz 53751-71379, Iran

[++]Present address: Donostia International Physics Center, P° Manuel Lardizábal 4, San Sebastián, Guipuzcoa 20018, Spain



**DOI: 10.1002/smll.202302355**

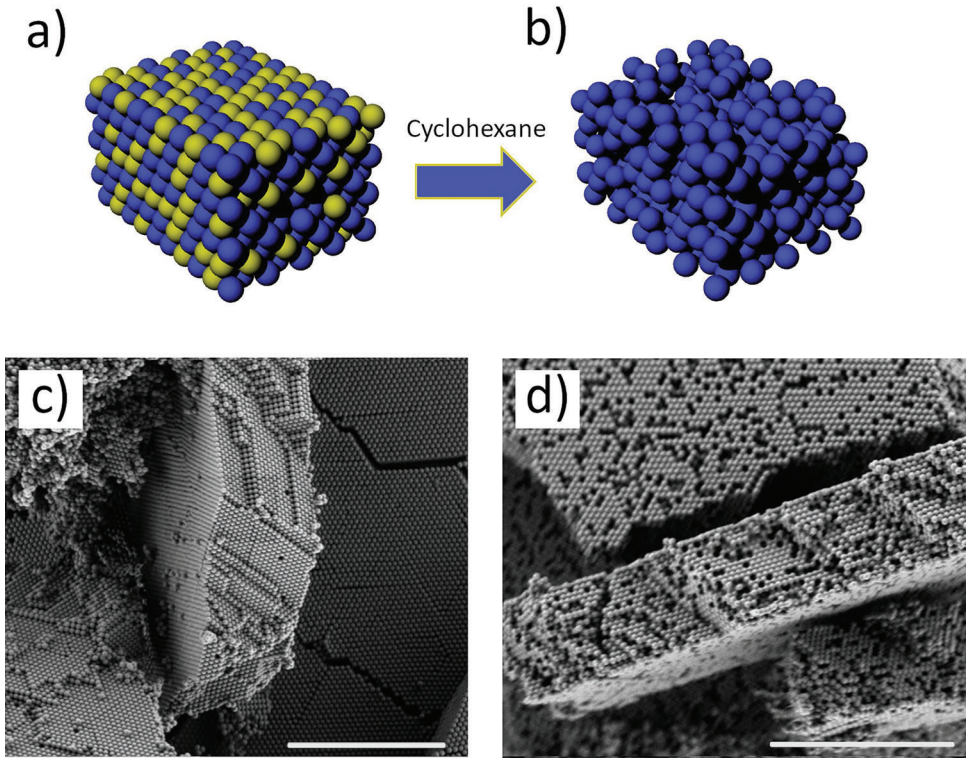


**Figure 1.** Schematic illustration of the binary self-assembled crystals a) before and b) after the removal of the doping spheres. SEM images of binary PhCs made of PMMA spheres of 334 nm c) before and d) after PS spheres are removed with cyclohexane. The scale bar in the SEM images is 10 µm.

In PhCs, the Fano's resonance appears in many systems in a natural way. Here, the narrow band is associated with the photonic band gap (Bragg peak) while the broadband, arising upon the perturbation of the system, can be brought about by an uneven background, either produced by Fabry–Perot oscillations[20] or by incoherent or Mie scattering.[21,22] In the latter case, the scattering is usually associated with disorder in the system and, therefore, it could be inferred that any kind of disorder introduced in the structure would give rise to asymmetric peaks in the spectra. However, geometrical disorder, whether in the form of polydisperse building blocks[23] or of a binary mixture of widely mismatched block sizes,[24,25] enhances light diffusion by the loss of lattice periodicity. As a consequence, the optical properties fade away leading to weaker but symmetric peaks in the spectra.[24] In contrast, as showed by Poddubny et al.,[26] Fano resonances can be observed in systems with compositional disorder, i.e., due to a variation in the dielectric constant of one of the components that form the structure.[27,28] The underlying reason is that geometrical disorder deteriorates the crystallinity of the structure leading to the extinction of the narrow band leaving only the diffusive, broadband channel available for transport. In contrast, compositional disorder alters both channels simultaneously, gradually degrading them and thus providing the characteristic asymmetry of the Fano resonance to the Bragg peak.

In this work, the optical properties of vacancy-doped PhCs are analyzed. These structures have been proved to be excellent archetypes for controlled insertion of random vacancies.[29] The asymmetric peaks obtained in reflectance spectra can be described as Fano resonances brought about by the interference between the photonic band gap reflection and the emerging background diffusion caused by vacancies and relying on the field enhancement at such defects. At a singular composition, signaled by the change of sign of the $q$ parameter, a structure emerges where Bragg reflectance not just decreases but completely vanishes. Herewith, we propose that the origin of such anomalous behavior is a consequence of both the singular electromagnetic field distribution in PhC's and their point defects. A simple model which considers the relative polarizability of the elements of a PhC and field enhancement in defects can account for such behavior. The final theoretical results closely resemble the experimental observations and give the guidelines to understand the electromagnetic response of defective PhCs.

## 2. Fabrication

Binary self-assembled crystals were built by the standard vertical deposition method,[30] where the building blocks used were monodisperse Polymethyl Methacrylate (PMMA) and Polystyrene (PS) spheres (acting here as dopants) of $D_s = 334$ and $D_d = 313$ nm of diameter respectively. The small difference in size (≈6%, just above the polydispersity) does not have any negative effect on the growth (see Figure S1, Supporting Information). Once the composite structures were achieved, **Figure 1**a, selective etching of the PS dopants yielded vacancy-doped crystals with a precisely controlled amount of vacancies from $\rho \approx 0\%$ to $\rho \gtrsim 38\%$, Figure 1b. The mechanical stability of the crystals was compromised above 38% vacancy, so we imposed this experimental limit in order to obtain reliable results. SEM inspection of

internal facets obtained by cleaving the samples reveals a binary face-centered cubic (fcc) structure before PS removal, Figure 1c, and a uniform distribution of vacancies inside the crystal after removal, Figure 1d. More details of the fabrication of the samples can be found elsewhere.[29]

## 3. Optical Characterization

Optical characterization was carried out by measuring both specular reflectance and transmittance in an IFS-66 Bruker Fourier Transform Infrared spectrometer at normal incidence (perpendicular to the opal (111) planes). For the sake of clarity, only reflectance will be discussed. The same results are obtained for the transmittance (see Figure S2, Supporting Information).

**Figure 2**a shows a contour plot compiled from the reflectance spectra taken at normal incidence as a function of wavelength and vacancy fraction in the range 0–38% vacancies for 20 layers thick structures, a safe choice of thickness that allows to assume the samples infinite.[31] Notice a continuous blue-shift of the Bragg peak due to the decrease in the effective refractive index of the structure as the number of vacancies increases. Different regions can be clearly identified at first sight from which representative spectra have been extracted and shown in Figure 2b. Reflectance spectra from Figure 2b can be fitted to Fano lineshapes according to the following general expression:

$$F\ (\tilde{\omega}) = A + B\frac{(\tilde{\omega} + q)^2}{1 + \tilde{\omega}^2} \quad (1)$$

where a single parameter, $q$, governs the asymmetry and the resonator strength. $A$ and $B$ are constants related to background and intensity, $\tilde{\omega} = 2(\omega - \omega_0)/\delta$ is the adimensional frequency related to the unperturbed resonance frequency, $\omega_0$ and the resonance width $\delta$.

Figure 2b shows reflectance spectra from self-assembled vacancy doped crystals at four representative vacancy concentrations (red lines) and their respective fits to a Fano lineshape (blue lines). Well below certain critical concentration ($\rho \ll \rho_c \approx 20\%$) a fairly clear Lorentzian profile (Figure 2b, $\rho = 0\%$) is obtained.

For low $\rho$ the intensity of the Bragg peak (centered around $\lambda_B = 740$ nm) is reduced as the number of vacancies increase. Samples belonging to this region present a behavior typical of PhCs with defects. A peak is measured corresponding to Fano lineshapes with $q \gg 1$. In this case, there is little or no contribution of scattering through the continuum. Therefore, the only possible transition is through the (modified) discrete state. This is consistent with previous work on diffusion,[5,32] and optical loss in PhCs.[33,34]

For $\rho$ from 10% to 19% (Figure 2b, $\rho = 13\%$), the intensity of the Bragg peak steadily decreases and the Fabry-Perot oscillations become fuzzy. Fitting to the Fano model bring $q$ parameters close to unity as the reflectance profile clearly turns asymmetric.[35]

For $\rho$ from 20% to 26%, a weak dip at the wavelength of the band gap can be seen (Figure 2b, $\rho = 26\%$) when parameter $q$ vanishes. In terms of optical properties, the net effect of disorder is that a band gap due to the band structure developed into a pass band where reflectance is almost fully inhibited. The unusual behavior adopted by the scattering can serve to mark the critical concentration.

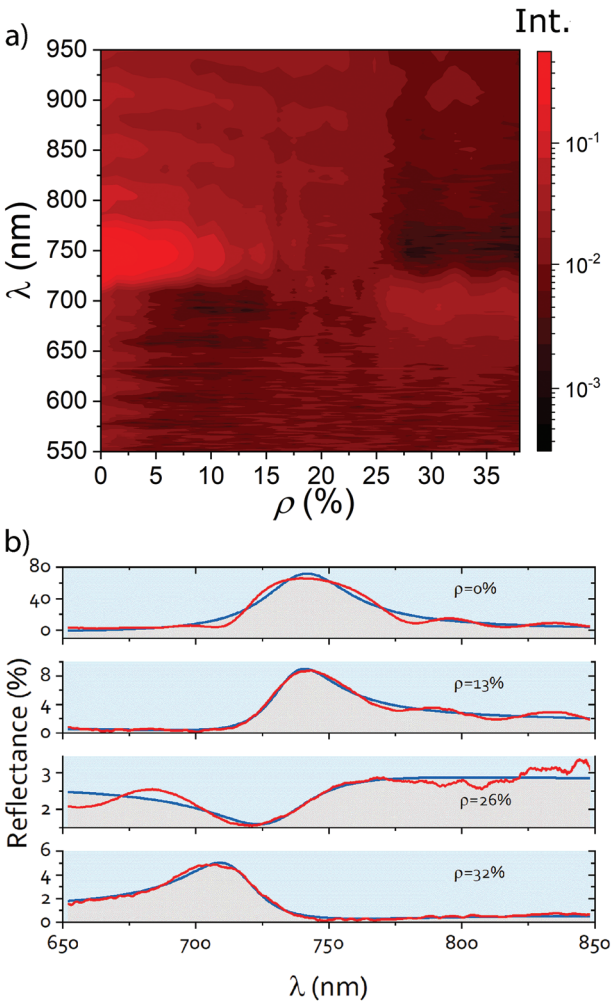


**Figure 2.** a) Specular reflectance of the vacancy doped crystals where the evolution of the photonic band gap is observed as the disorder of the structure increases. The asymmetric Bragg peak vanishes for $\rho = 20$–$25\%$ to recover the asymmetry for higher percentages of vacancies. b) Reflectance spectra (red line) and the fit (blue line) to the Fano line-shape at the band gap for a) 0%, b) 13%, c) 26%, and d) 32%. Different symmetric or asymmetric profiles are obtained depending on the percentage of vacancies. All the spectra are from 20-layers thick samples.

Above 26% an asymmetric profile is recovered that tends back to Lorentzian in profile for concentrations far above the critical ($\rho > \rho_c$). Notice that the peak is the mirror image of that below threshold with the relative maxima and minima positions exchanged (Figure 2b, $\rho = 32\%$). This lineshape change can be obtained simply through a change of sign in the $q$ parameter of the Fano resonance only when $q$ is small. This singular system, in which spheres are removed without altering the lattice parameter, preserves band gap features even for a high percentage of the vacancies.

One of the most remarkable features of the disorder present in this system, at variance with disorder induced by polydispersity of the spheres is that, here, long-range correlation is preserved.

We identify the narrow Fano channel with the photonic band gap (Bragg diffraction) whereas the broad continuum is

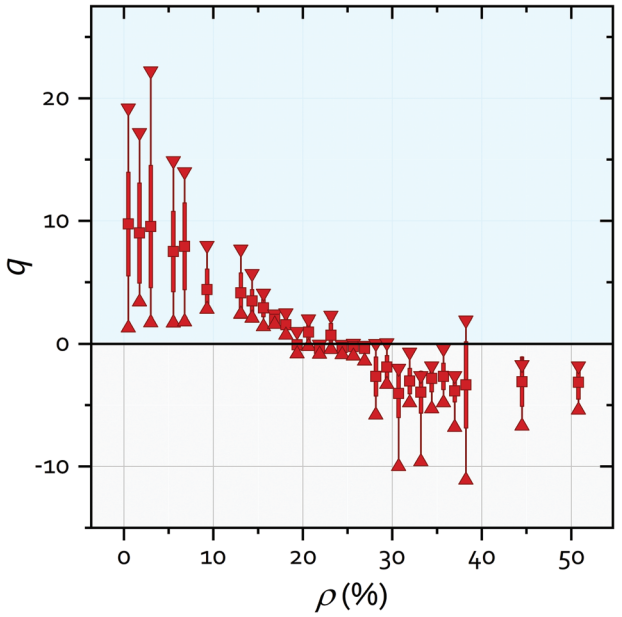


**Figure 3.** Fano's $q$ parameter. Experimental values: squares are average over sample thicknesses, bars span one standard deviation and pointed triangles cover the whole range of values encountered.

originated by the background scattering, i.e., by lattice defects that cause diffuse light scattering. In the case of a regular geometrical arrangement of spheres, two types of scattering can be expected. On the one hand, diffuse scattering arises from the interaction of electromagnetic waves with a medium comprising different refractive indices like in an alloyed colloidal crystal[36] or different sizes.[24] On the other hand, frustrated Fabry–Perot interference can be caused if a number of lattice sites are absent disrupting the index periodicity like in this case. This latter contribution is exclusive of periodic structures (like PhC's) and appears when defects modify the optical path preventing coherent interference.

The behavior just described can be seen in **Figure 3** that summarizes the results for the $q$ parameter obtained from the fittings of experimental spectra as in Figure 2 to the Fano Equation (1) for doped crystals of up to 35 monolayers. This type of representation is most appropriate since it consolidates data spread due to both the normal statistical dispersion and thickness dependence. The squares are the mean values, the solid bars mark one standard deviation from the mean values, and inward pointing triangles cover the full data spread. Notice that samples thinner than $\lambda_B$ always produce an underestimate of $q$ even for low vacancy concentrations. It has been commonly understood that bands can be seen as emerging from sphere resonances as electronic bands emerge from atomic levels. This was first studied by computing the DOS in an fcc structure as a function of packing fraction to observe that pseudogap is as a remnant of the single-sphere Mie resonances.[37] When the crystal is in the early stages of growth (thin layers) the Bragg peak is forming and the corresponding resonance narrowing and strengthening (see Figure S3, Supporting Information). The minimum values, very close to zero, are always observed to arise from the thinnest samples.

## 4. Modeling

In order to shed light on the behavior of the reflectance one may normally resort to two types of approaches. The obvious one is to numerically solve the Maxwell equations by FDTD. However, this approach is severely limited by CPU and memory constrains when multiple defects are to be considered since large supercells would be needed. Therefore, such kind of calculations cannot be used to but the simplest instances of this system, and we have limited those to selected configurations. Instead, we have resorted to an analytical model where the crystal is simulated by representing the periods of PhC by a set of dipoles in a Bravais lattice. For simplicity, we assume a one-dimensional string like columns in Figure S4 (Supporting Information). Each element of the column corresponds to a unit cell of the PhC structure of a length given by $D$ and a volume $V_c \propto D^3$. In the case of the perfect crystal, the chain is composed by two types of regions with different polarizability or dielectric constant, $\epsilon$. Those with the largest permittivity, $\epsilon_s$, corresponds to the PhC *spherical* particles (deep yellow in Figure S4, Supporting Information), while those with $\epsilon_v$ represent the *voids* of the crystalline structure (light yellow in Figure S4, Supporting Information). Dielectric contrast between them, along the periodic structure, produces Bragg reflections in perfect crystals. On this structure, we introduce vacancies at random replacing the pair ($\epsilon_s$, $\epsilon_v$) making up normal cells with whole empty cells, with dielectric constant $\epsilon_d$ (light yellow cells in Figure S4, Supporting Information) and average over many realizations. In our particular case, we consider that, the refractive index of voids in ordinary cells is identical to that of the vacancies, as both media are filled with air, that is, $\epsilon_{v\,=}\,\epsilon_d$. In this way, we can introduce different dielectric polarizations for each region. Considering the relative sizes of the spheres, $fV_c$, and $(1-f)V_c$, correspond respectively to the volume occupied by spheres and voids, being $f \approx 0.74$ is the filling fraction of the fcc crystalline structure. Using Clausius–Mossotti we can approximate the static polarizabilities of each component of the model:[38]

$$\alpha_s = \varepsilon_0\, V_d f \frac{\varepsilon_s - \langle\varepsilon\rangle}{\varepsilon_s + 2\langle\varepsilon\rangle}$$

$$\alpha_v = \varepsilon_0\, V_c \left(1-f\right) \frac{\varepsilon_d - \langle\varepsilon\rangle}{\varepsilon_d + 2\langle\varepsilon\rangle}$$

$$\alpha_d = \varepsilon_0\, V_c \frac{\varepsilon_d - \langle\varepsilon\rangle}{\varepsilon_d + 2\langle\varepsilon\rangle} = \frac{\alpha_v}{\left(1-f\right)} \tag{2}$$

The latter expression includes the relationship between the voids and defects polarizabilities: $\alpha_v = (1-f)\,\alpha_d$. All the three polarizations are expressed as a function of an effective dielectric constant of the medium $\langle\epsilon\rangle$. To calculate it we have employed the Bruggemann model[39] that binds every component's filling fraction and dielectric function: $(1-\rho)f$ and $\epsilon_s$ for spheres; $(1-\rho)(1-f)$ and $\epsilon_d$ for voids; $\rho$ and $\epsilon_d$ for vacancies, in a single expression.

$$(1-\rho) f \frac{\varepsilon_s - \langle\varepsilon\rangle}{\varepsilon_s + 2\langle\varepsilon\rangle} + (1-\rho)\left(1-f\right) \frac{\varepsilon_d - \langle\varepsilon\rangle}{\varepsilon_d + 2\langle\varepsilon\rangle} + \rho \frac{\varepsilon_d - \langle\varepsilon\rangle}{\varepsilon_d + 2\langle\varepsilon\rangle} = 0 \tag{3}$$

If the dielectric polarizations are known, the total dipolar field can be computed by averaging over of $N$-cell strings with the corresponding cell polarizability $\tilde{\alpha}_i$. In the simplest approximation,

a plane wave travelling along the $Z$ direction that impinges on a string of dipoles lying on the $Z$-axis will be reflected creating a field at $z = -\infty$ given by:

$$E_r \propto \sum_{i=1}^{N} \frac{p_i}{z_i} e^{-2\imath k z_i} \approx \frac{1}{h} \sum_{i=1}^{N} p_i e^{-2\imath k z_i} \tag{4}$$

with $\imath$ the imaginary unit, $p_i$ and $z_i$ the $i$th dipole and its position; $k = 2\pi/\lambda$ being the wave number in vacuum of the incoming radiation and $h$ the distance to the detector.

The induced dipole can be written as $p_i = \tilde{\alpha}_i \; E(z_i)$ as a function of the local field which, in turn, can be expressed as $E(z_i) = \gamma_i \; E_0(z_i)$ in terms of the incident radiation with $\gamma_i$ a factor allowing for the field enhancement in case the $i$th position is empty which constitutes a microcavity in a PhC. Thus $\gamma_i = \gamma$ for defects (vacancies or empty cells) and $\gamma_i = 1$ for full cells. Therefore, the effective polarizability of defects is given by: $\tilde{\alpha}_d = \gamma \alpha_d$.

Since we have so far only considered static polarizability, in the summation of Equation (4) the different phases of the dipoles in the unit cell of the PhC must be introduced. When calculating the dielectric response of the occupied cells, the delay originating in the high (sphere) and low (vacuum) refractive index regions is shifted by an amount $\Lambda \approx D/2$, where $D$ is the sphere size. We introduce an effective complex polarizability for the whole cell $\tilde{\alpha}_s$ as:

$$\tilde{\alpha}_s = \alpha_s \; + \alpha_v e^{\imath k n_s \Lambda} \tag{5}$$

In this equation we have distinguished between dielectric polarization of different dielectric elements and the full electromagnetic polarization of each cell in the PhC by using the tilde sign "˜" for the latter.

Thus, with probability $\rho$, a cell is empty (vacancies) presenting polarizability $\tilde{\alpha}_d$, which represent the *dopants*; otherwise, it will present polarizability $\tilde{\alpha}_s$.

Since in a crystal the dipoles are immersed in a material medium, when computing the phase, the optical paths across a scatterer and a dopant must be considered and are given by their optical sizes, $d_s = D\, n_s$ and $d_d = D\, n_d$ respectively. Therefore, the optical paths are given by:

$$z_i = \frac{1}{2} \; \left(d_1 + d_i\right) + \sum_{j>1}^{i-1} d_j \tag{6}$$

Notice that, even when both defect and occupied sites are of the same size (required for good crystalline quality) their optical size is different and this is one of the sources of the modification of the Fano profile of the Bragg reflection.

In order to compute Equation (4) the following cases should be considered. If two random particles are next-nearest neighbors the optical path from center to center is given by $d_s$ with probability $(1-\rho)^2$ (scatterer-scatterer), $d_d$ with probability $\rho^2$ (dopant–dopant) or $\frac{(d_s+d_d)}{2}$ with probability $2\rho(1-\rho)$ (scatterer–dopant or dopant–scatterer).

The reflected intensity, $I \propto \mathbf{E}_r^* \cdot \mathbf{E}_r$, is given by

$$I \propto \sum_{i=1}^{N} \left|\tilde{\alpha}_i\right|^2 + 2 \sum_{i=1}^{N} \sum_{j>i}^{N} \tilde{\alpha}_i^* \tilde{\alpha}_j \cos\left(2k\left(z_j - z_i\right)\right) \tag{7}$$

where $\tilde{\alpha}_i = \tilde{\alpha}_s$ with probability $1-\rho$ (a scattering cell) and $\tilde{\alpha}_i = \tilde{\alpha}_d$ with probability $\rho$ (a dopant, empty cell).

Let us now consider the average over many different $N$-dipole strings. Each of them will have different random distributions of dopants but with the same dopant density and all of them will incoherently contribute to the backscattering. That is, let's assume that for each sample region (columns in Figure S4, Supporting Information) the field is the vector sum from the stacked dipoles' contributions (according to their phase) and that regions contribute to the intensity independently. Then, the reflected intensity will be given by averaging over many realizations of the summation in Equation (7):

$$\langle I \rangle \propto \left\langle \sum_{i=1}^{N} \left|\tilde{\alpha}_i\right|^2 \right\rangle + 2 \left\langle \sum_{i=1}^{N} \sum_{j>i}^{N} \tilde{\alpha}_i^* \tilde{\alpha}_j \cos\left(2k\left(z_j - z_i\right)\right) \right\rangle \tag{8}$$

which, using the definition of covariance between two random variables (see Supporting Information) can be separated in two terms $\langle I \rangle \propto I_{sym} + I_{cov}$ with designations (*symmetric* and *covariance*) justified below:

$$I_{sym} = \left\langle \sum_{i=1}^{N} \left|\tilde{\alpha}_i\right|^2 \right\rangle + 2 \sum_{i=1}^{N} \sum_{i<j}^{N} \langle \tilde{\alpha}_i^* \tilde{\alpha}_j \rangle \langle \cos[2k(z_i - z_j)] \rangle \tag{9}$$

and

$$I_{cov} = \; 2 \sum_{i=1}^{N} \sum_{j>i}^{N} \mathrm{cov}\left\{\tilde{\alpha}_i^* \tilde{\alpha}_j, \cos\left[2k\left(z_i - z_j\right)\right]\right\} \tag{10}$$

Considering the statistical distribution of a number of vacancies in a stack it is possible (see Supporting Information) to arrive at an analytical expression for the random optical paths needed to compute the phases that provide an analytical expression for both terms giving:

$$I_{sym} = \; N\langle|\tilde{\alpha}|^2\rangle + 2|\langle\tilde{\alpha}\rangle|^2 \sum_{i=1}^{N} \sum_{j>i}^{N} (1-\rho)^2 T_{ss}^{ij}(k) + \rho^2 T_{dd}^{ij}(k)$$

$$+2\rho\,(1-\rho)\; T_{sd}^{ij}(k) \tag{11}$$

with the three $T$ parameters depend only on the $i$–$j$ distance ($i$–$j$–1) and carry the dependence on wavelength, geometrical features, and the concentration of vacancies (see Supporting Information).

In the particular case of the symmetric contribution further simplification can be had for $d_d/d_s \approx 1$ where $I_{sym}$ term can be approximated by the familiar functional form:

$$I_{sym} \approx N\sigma_\alpha^2 + |\langle\tilde{\alpha}\rangle|^2 \left[\frac{\sin Nkd}{\sin kd}\right]^2 \tag{12}$$

with $d \equiv \langle d \rangle = (1-\rho)\; d_s + \rho d_d$ the average optical size; $\sigma_\alpha^2 = \langle|\tilde{\alpha}|^2\rangle - |\langle\tilde{\alpha}\rangle|^2$, the polarizability variance; and $|\langle\tilde{\alpha}\rangle|^2 = (1-\rho)^2\; |\tilde{\alpha}_s|^2 + \rho^2 |\tilde{\alpha}_d|^2 + 2\rho(1-\rho)\Re(\tilde{\alpha}_s \tilde{\alpha}_d^*)$.

$I_{sym}$ contains a constant background intensity, proportional to the variance of the polarizability, plus the Bragg diffraction lineshape coming from a homogenous PhC with polarizability and

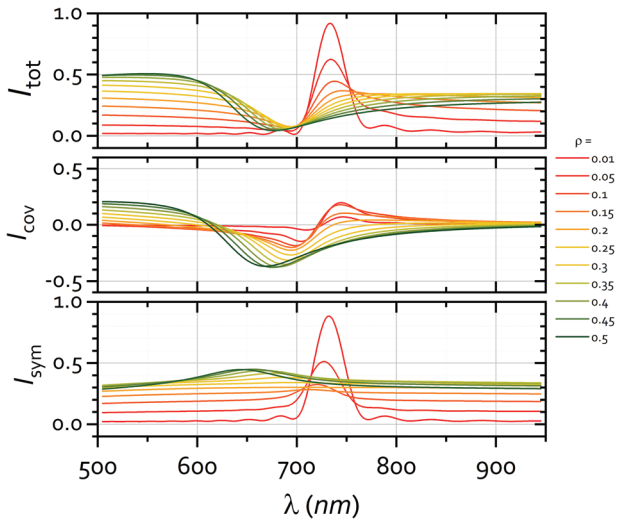


**Figure 4.** Computed spectra. The symmetric, covariant a total reflectance as a function of wavelength or various defect densities considering $\gamma = 3$. Notice how the background in $I_{sym}$ (reflectance outside the Bragg peak) increases with disorder allowing for a negative contribution in $I_{cov}$ to bring the total to near cancellation.

particle optical size given by the averaged values. This is the typical spectrally *symmetric* response of a regular periodic structure hence the designation, see **Figure 4**.

The second term ($I_{cov}$) arises from the *covariance* between phases' differences and polarizabilities' products in the dipoles' column, hence the designation. Both quantities are correlated because the phase at an element in the stack depends on how many constituents of each kind (scatterers or dopants) there are underneath. Using the definition of covariance as the average of the products of fluctuations around the mean (see Supporting Information) leads to:

$$I_{cov} = 2\sum_{i<j}(1-\rho)^2\left(\left|\tilde{\alpha}_s\right|^2 - \left|\langle\tilde{\alpha}\rangle\right|^2\right)T_{ij}^{ss}(k) + \rho^2\left(\left|\tilde{\alpha}_d\right|^2 - \left|\langle\tilde{\alpha}\rangle\right|^2\right)T_{ij}^{dd}(k) + 2\rho(1-\rho)\left(\Re\left(\tilde{\alpha}_s^*\tilde{\alpha}_d\right) - \left|\langle\tilde{\alpha}\rangle\right|^2\right)T_{ij}^{sd}(k) \quad (13)$$

This contribution to the reflectance is a function that inverts its asymmetry when $|\langle\tilde{\alpha}\rangle|^2$ reaches a minimum, like a Fano function does when $q$ goes to zero, where it adopts an inverted Lorentzian lineshape (see Figure 4).

Once the polarizabilities and defect density have been set, we can plot the value of $(I_{sym} + I_{cov})/(N^2\alpha_s^2)$ versus $\lambda$. In Figure 4 we have plotted contributions from both $I_{sym}$ and $I_{cov}$ to the total backscattered intensity for $\gamma = 3$. The calculated reflected intensity is very similar to that found experimentally for the vacancy-doped PhC. The Lorentzian Bragg diffraction found for light doping, $\rho \approx 0$, turns into a Fano-like response with $q \gg 0$. Then, for $\rho \approx \rho_c$ it assumes a $q \approx 0$ and changes sign. For further doping, $\rho > \rho_c$, the line recovers the Lorentzian shape with $q < 0$.

This illustrates the fact that the $q$ parameter behavior strongly depends on the density of vacancies due to the change on the behavior of the covariance versus wavelength. Notice that, without considering the covariance only a maximum can be obtained.

The value of $q$ can be interpreted as the ratio of the discrete state-mediated transition rate to that mediated by the continuum of states. It derives from the strength of the interaction with the perturbation introduced by the continuum in the perturbative approximation of the original quantum formulation.[12] In our case, it is governed by the concentration of the vacancies in the opals and a value of zero points to total dominance of non-resonant scattering as opposed to photonic band-mediated scattering where $q$ would tend to infinity.

## 5. Critical Concentration

According to Equation (12), apart from a background term, the factor $|\langle\tilde{\alpha}\rangle|^2$ determines the strength of the wavelength dependent term in $I_{sym}$. Therefore, we can expect, to a good degree of approximation, that the defect concentration which minimizes $|\langle\tilde{\alpha}\rangle|^2$ will make Bragg diffraction peak disappear. As a consequence, the intensity curve $I_{cov}$ adopts a dip corresponding to a $q = 0$ Fano profile. This critical concentration is the solution to:

$$\frac{d|\langle\tilde{\alpha}\rangle|^2}{d\rho} = 0 \quad (14)$$

According to Equation (5) the explicit expression of $|\langle\tilde{\alpha}\rangle|^2$is given by $|\langle\tilde{\alpha}\rangle|^2 = |(1-\rho)(\alpha_s + \alpha_v e^{ikn_s\Lambda}) + \rho\gamma\alpha_d|^2$ so that, at the Bragg maximum, $k = \frac{\pi}{d}$ the minimum condition in Equation (14) is given by:

$$\rho\left(\alpha_s^2 + \alpha_v^2 + \alpha_s^2\gamma^2 - 2\alpha_s\alpha_d\gamma + 2\alpha_v\left(\alpha_s - \alpha_d\gamma\right)\cos\frac{\pi\Lambda}{d}\right) = \alpha_s^2 + \alpha_v^2 - \alpha_s\alpha_d\gamma + \alpha_v\left(2\alpha_s - \alpha_d\gamma\right)\cos\frac{\pi\Lambda}{d} \quad (15)$$

Additionally, another condition can be obtained from the equation of the effective medium for the dielectric constant, as the Bruggemann model (Equation (3)) requires by definition that the effective static polarizability be zero. So that, considering of Equation (2), Equation (3) can be written as

$$(1-\rho)\alpha_s + \left(1 - f + \rho f\right)\alpha_d = 0 \quad (16)$$

With the definitions in Equations (2), (15), and (16) it is possible to define a system of two equations in $\rho$ and $\gamma$, resulting in a relationship between the field enhancement at the defects, represented by $\gamma$, and the critical defect density $\rho_c$, given by the expression:

$$\rho_c = \frac{(1-f)(2f-\gamma-1)\left(1-\cos\frac{\pi\Lambda}{d}\right)}{1 + 2f^2 + \gamma^2 - 2f(1+\gamma) - 2(1-f)(\gamma-f)\cos\frac{\pi\Lambda}{d}} \quad (17)$$

Now the reflectance curve becomes a minimum at the Bragg wavelength. It is worth to note that the critical defect density does not depend on the polarizability but on geometric parameters and on the field enhancement factor. Substituting $f = 0.74$ and

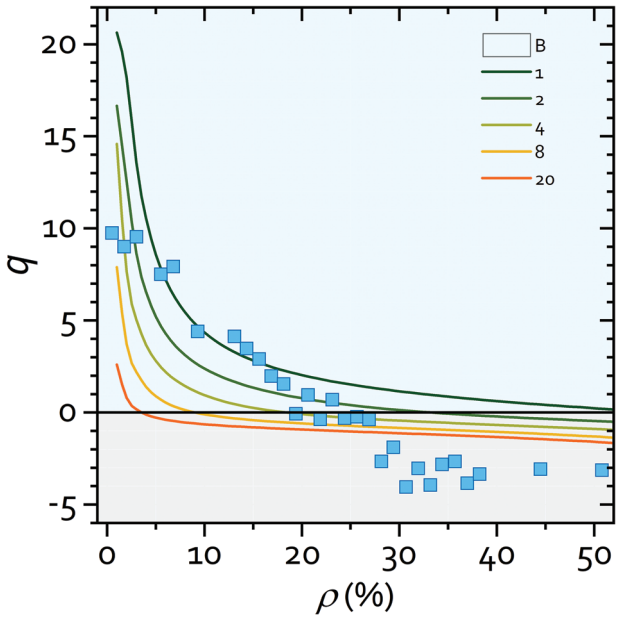


**Figure 5.** Fano's $q$ parameter. Symbols correspond to experimental average values as in Figure 3. Fano parameters obtained by fitting the spectra in Figure 4 are plotted here as solid lines for several values of $\gamma$.

$\Lambda = D/2$ we get an explicit expression for the critical density:

$$\rho_c = \frac{0.260\gamma - 0.125}{\gamma^2 - 1.480\gamma + 0.615} \tag{18}$$

that shows that as the enhancement grows the critical concentration of vacancies notably reduces (see in Figure S4).

Using Equations (11) and (13) and assuming vacancy density independent enhancement, it is possible to compute the reflectance spectra and, by fitting, the Fano's $q$ parameter as a function of $\rho$.

Results are plotted in **Figure 5** (solid color lines) for several values of $\gamma$. Note how, in agreement with the experimental results, the model predicts a crossover form positive to negative values of the $q$ parameter as the density of vacancies increases. To keep the model as simple as possible we have considered a constant value of $\gamma$, affecting only to the dopants. However, from Figure 5, it is clear that a more elaborated dependence with the density is needed in order to quantitative reproduce the experimental results.

As can be seen, all dependence of the critical density is on the field enhancement, which, in turn, will mostly depend on the refractive index contrast. Note how, if $\gamma = 1$ (no field enhancement) the critical density is equal to one: homogeneous medium. In other words, Bragg band inversion in vacancy-doped PhC's is an indirect effect of the field enhancement in defect sites.

## 6. Field Enhancement

At this point, we wish to provide an estimate of the field enhancement in defects at the Bragg band. Light with wavelength in the Bragg band cannot propagate in the crystal. However, defects create localized states that open channels for propagation. Therefore, the field inside a defect, $E_d$, (empty space left by a missing sphere) should be much larger than in the small (octahedral and tetrahedral) voids, $E_v$, (always empty) in the perfect PhC. In order to check this hypothesis, we modelled a finite PhC by FDTD. Details can be found in the Supporting Information.

Using the 3D field amplitude in the perfect and defective PhC, it is possible to compute $\gamma$. The definition of $\gamma$ considers the ratio of field enhancement at defect loci, with dielectric constant $\epsilon_d$ with respect to that of voids at perfect PhC, with the same dielectric constant $\epsilon_v = \epsilon_d$. So that, according to this definition its average $\langle\gamma\rangle$ can be calculated as:

$$\langle\gamma\rangle = \frac{\int_{C_d} E_d dv}{\int_v E_{v,\mathrm{PhC}} dv} \tag{19}$$

In this expression we considered that the incident field of Equations (4) and (7) $E_r$ is linearly polarized (perpendicular to the $z$-axis), so that the coherent interference of the internal field will only take place with the parallel component to $E_r$ so that $E_r \| E_d$. The integrals in Equation (19) are computed in the volume of a single cell containing one defect ($C_d$) and the voids completing the unit cell ($V_c$), respectively. That is, the amplification factor is given by the ratio between the average electric field in the empty volume left by a removed sphere and the field averaged in its associated voids in a perfect PhC. **Figure 6** summarizes the results for five wavelengths around the Bragg center (717 nm for the particular simulation).

This simple calculation indicates that outside the Bragg condition, the amplification factor is modest, but right at the Bragg wavelength, it can reach values of $\langle\gamma\rangle = 3$. Such enhancement is mostly due to the fact that, in a perfect PhC at the spectral region of the bandgap, the field distribution follows a periodic pattern. However, when a defect appears, it can be seen how the field at the defect resembles that of the perfect crystal, so that at the defect position, the field is quite similar to that of an occupied position. This behavior does not take place in case of a quasistatic approximation, and this fact seems to be the responsible of the Bragg maximum inversion.

This enhancement factor may change with defect concentration, growing smaller as the defect concentration increases. However, one can expect that, when defects are few and far between, this value will be high but the crystal average will not much differ from 1. Let's not forget that $\gamma$ depends on the number of vacancies in the defect, their shape, the average dielectric function of their environment and their relative abundance. Regarding the latter, size, shape, and amount greatly increase for large vacancies concentration,[29] rendering its contribution highly nontrivial and difficult to grasp with our simple model. This fact is probably the main reason behind poorer fitting for higher $\rho$. In addition, for concentrations larger that the critical value, continuous paths of defects can be expected that extend throughout the PhC. This seems to be closely linked with percolation theory where this event is expected at $\rho_c = 0.18$.

In this regions, two opposite mechanism compete. On the one hand, defects and the high field regions associated to them may coalesce, decreasing the net polarization of the whole PhC. On the other hand, field enhancement is expected to diminish, as it depends on the "average" contrast between different phases. In this regard, the band inversion associated to a change of sign of

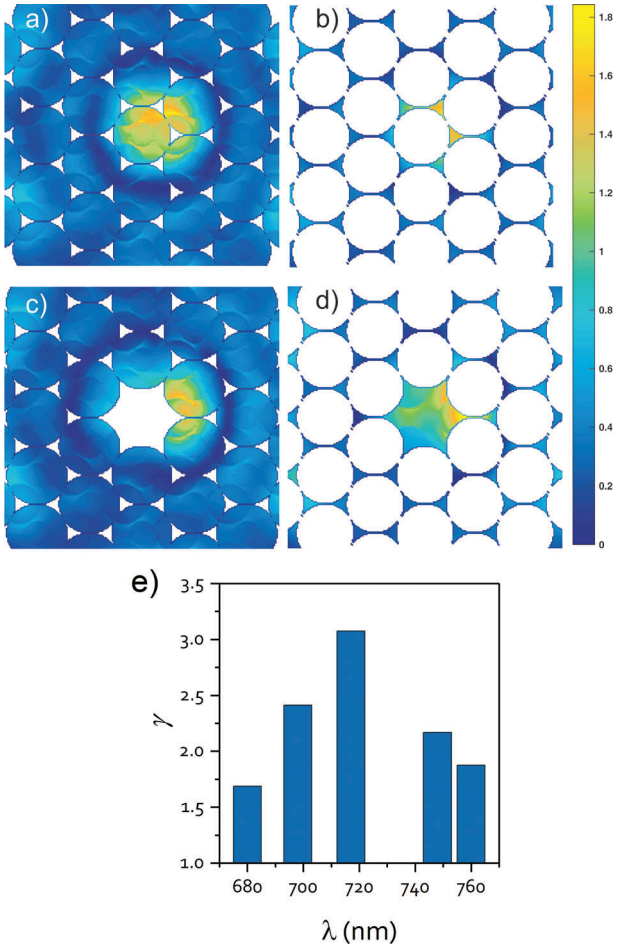


**Figure 6.** Field a) inside and b) outside the spheres, in c,d) the case where the structure is the PhC, and when one sphere is missing. The enhancement in Equation (18) is the ratio of the average field intensity around the center sphere in (b) and the missing sphere in (d). e) Field enhancement measured as the ratio of the field at the center of a missing dielectric sphere (vacancy) to that in the empty space surrounding a present sphere for various wavelengths around the Bragg wavelength $\lambda_B = 717$ nm.

$q$, can be rationalized as the condition when the effective polarization is zero. If so, the interaction causing the resonance disappears. From an electromagnetic point of view, fields may propagate even at the Bragg condition. But, as field inside defects is amplified, the material presents an enhanced transmission. In fact, this is the condition for manufacturing an invisible metamaterial. It should be noted, that at the $q$ =0 condition, the reflectance minimum is very close to zero, so that the transmission (assuming no losses) is $T = 1 - R \approx 1$.

For larger concentrations, $\gamma$ will progressively be smaller, as the high dielectric phase becomes scarce, so that Bragg inversion gradually tends to disappear. However, covariance-driven band asymmetry remains resulting in a negative $q$.

## 7. Discussion

The observed data and the theoretical models indicate that vacancy doped PhC's constitute the first systems where doping decreases average refractive index (by removing material) and thus present a series of linked unusual phenomena also found in similar systems. In fact, the effect of vacancies in sphere PhC's has been previously well established and there is plenty of references in the literature where vacancies are used to create microcavities.[40] Usually, a single and isolated defect introduces a forbidden electromagnetic state into the bandgap which is associated to a field localization which can be observed as a dip in the Bragg reflection peak. As the spectral position of this dip depends on the defect details, a statistical distribution of defects produces a reduction and broadening of the Bragg band. We have assimilated this feature at low vacancies concentration as an increase of the damping term of the Fano-like Bragg band profile. When the defects start to be abundant, they remove dielectric spheres, the high permittivity component, in appreciable proportions. This, in turn, lowers the average polarizability and, according to Equation (12), reflection, beside causing a blue shift in the Bragg. However, at a critical defect concentration, the Bragg peak not only loses intensity but it transforms into a minimum. This unintuitive result for dielectric spheres and air PhC has nevertheless been found in PhC's, in which the low refractive medium is filled with a material to fully cancel the dielectric contrast. This result can be rationalized by considering that when both refractive indices are identical, light propagates as a plane wave because the medium is optically homogeneous.

The theoretical model here used reproduces the same features of PhC's with two matching dielectric materials, but at the expense of introducing the defect local field enhancement hypothesis.

In this sense, the local field enhancement is the key to understand the strange behavior of defective PhCs. In this case, nor the refractive index matching supresses the Bragg peak, but the enhanced field inside the vacancies do. Additionally, vacancies break optical coherence so that they considerably increase the scattering contribution. These features modify the Fano curve, decreasing the $q$ parameter (as a consequence of reduction of polarization and field enhancement) and increasing $\gamma$ (due to incoherent scattering). However, those effects are not linear as defect concentration increases because the PhC crystalline structure is substantially modified as well as the electromagnetic field distribution. Consequently, the Bragg resonance in a defective PhC can be described by Fano curves with non-linear behavior versus defects concentration. When a critical concentration of defects is achieved, internal electric fields cancel the effect of the external one, giving place to a reflectance minimum.

## 8. Conclusions

In conclusion, in this work we have studied the variation of optical properties in PhCs with fine control over vacancies composition. Fano-like resonances manifest in the optical reflectance spectra. Not only have we achieved all the different asymmetric profile characteristics of the Fano resonance, but we have also set a correlation between the $q$ parameter and the percentage of vacancies. We have presented a simplified model based on the single scattering from a two components system capable of mimicking the experimental results. The fundamental role played by the covariance in this model has two important implications. The first is that in order to find non-symmetric responses, a low

transversal coherence is required. And the second, that the field localization in PhC defects must be taken into account. Under this hypothesis, the experimental results can be fairly accounted for. In other words, we can say that defects have two main effects in the optical properties of PhC. On the one hand, they reduce the average effective static polarizability of the medium, so that the Bragg peak reduces its intensity. On the other hand, and in a more quantitative way, it can be said that Fano process reduces the resonant part, $q$, and increases the damping $\gamma$. However, and due to the field enhancements at defects, their role in the electromagnetic response of the PhC is substantially larger than would correspond to a mere "rule of mixtures" law. Therefore, for defects concentrations around $\rho = 0.2$, the total contribution of defects is similar to the remaining 80% of dielectric spheres.

To conclude, it is worth to mention that this phenomenon resembles the well-known extraordinary transmission, where interaction between resonances results in large field enhancements as has been described in subwavelength plasmonic structures.[41] In both cases, the systems may be considered invisible metamaterials as they do not reflect light at the critical condition.

## 9. Experimental Section

Experimental details and any associated references are available in the Supporting Information.

## Supporting Information

Supporting Information is available from the Wiley Online Library or from the author.

## Acknowledgements

This work was partially funded by the Spanish PID2021-124814NB-C21, PGC2018-095777-B-C22, PID2019-109905GA-C22, the "María de Maeztu" Programme for Units of Excellence in R& D (CEX2018-000805-M), the UAM-CAM project (SI1/PJI/2019-00052) projects. The authors thankfully acknowledge N. de Sousa for fruitful discussions.

## Conflict of Interest

The authors declare no conflict of interest.

## Data Availability Statement

The data that support the findings of this study are available from the corresponding author upon reasonable request.

## Keywords

correlated disorder, disorder, Fano resonance, photonic crystals, vacancy doping

Received: March 20, 2023
Revised: May 12, 2023
Published online: June 6, 2023

[1] M. Buchanan, *Nat. Phys.* **2019**, *15*, 203.
[2] V. I. Kukulin, V. M. Krasnopol'sky, J. Horáček, in *Theory of Resonances*, Springer Netherlands, Dordrecht, **1989**, pp. 302.
[3] S. J. Peale, *Annu. Rev. Astron. Astrophys.* **1976**, *14*, 215.
[4] E. B. Davies, *Proc.: Math., Phys. Eng. Sci.* **1999**, *455*, 585.
[5] S. P. Shipman, in *Prog. Comput. Phys. Vol. 1: Wave Propag. Period. Media*, Bentham Science Publishers, UAE, **2012**, pp. 7–49.
[6] A. I. Kuznetsov, A. E. Miroshnichenko, M. L. Brongersma, Y. S. Kivshar, B. Lukyanchuk, *Science* **2016**, *354*, 2472.
[7] S. Gottardo, R. Sapienza, P. D. García, Á. Blanco, D. S. Wiersma, C. López, *Nat. Photonics* **2008**, *2*, 429.
[8] W. Zhu, T. Xu, H. Wang, C. Zhang, P. B. Deotare, A. Agrawal, H. J. Lezec, *Sci. Adv.* **2017**, *3*, e1700909.
[9] D. Bischof, F. Kehl, M. Michler, *Opt. Commun.* **2016**, *380*, 273.
[10] T. Wood, M. Naffouti, J. Berthelot, T. David, J. B. Claude, L. Métayer, A. Delobbe, L. Favre, A. Ronda, I. Berbezier, N. Bonod, M. Abbarchi, *ACS Photonics* **2017**, *4*, 873.
[11] Y. S. Joe, A. M. Satanin, C. S. Kim, *Phys. Scr.* **2006**, *74*, 259.
[12] U. Fano, *Phys. Rev.* **1961**, *124*, 1866.
[13] A. E. Miroshnichenko, S. Flach, Y. S. Kivshar, *Rev. Mod. Phys.* **2010**, *82*, 2257.
[14] M. F. Limonov, M. V. Rybin, A. N. Poddubny, Y. S. Kivshar, *Nat. Photonics* **2017**, *11*, 543.
[15] S. Yuan, X. Qiu, C. Cui, L. Zhu, Y. Wang, Y. Li, J. Song, Q. Huang, J. Xia, *ACS Nano* **2017**, *11*, 10704.
[16] G. Cao, S. Dong, L. M. Zhou, Q. Zhang, Y. Deng, C. Wang, H. Zhang, Y. Chen, C. W. Qiu, X. Liu, *Adv. Opt. Mater.* **2020**, *8*, 1902153.
[17] Z. He, W. Xue, W. Cui, C. Li, Z. Li, L. Pu, J. Feng, X. Xiao, X. Wang, G. Li, *Nanomaterials* **2020**, *10*, 687.
[18] N. S. King, L. Liu, X. Yang, B. Cerjan, H. O. Everitt, P. Nordlander, N. J. Halas, *ACS Nano* **2015**, *9*, 10628.
[19] Y. Yu, W. Xue, E. Semenova, K. Yvind, J. Mork, *Nat. Photonics* **2017**, *11*, 81.
[20] D. R. Abujetas, M. A. G. G. Mandujano, E. R. Méndez, J. A. Sánchez-Gil, *ACS Photonics* **2017**, *4*, 1814.
[21] M. V. Rybin, A. Khanikaev, M. Inoue, K. Samusev, M. Steel, G. Yushin, M. F. Limonov, *Phys. Rev. Lett.* **2009**, *103*, 023901.
[22] P. Markoš, V. Kuzmiak, *Phys. Rev. A* **2016**, *94*, 033845.
[23] R. Rengarajan, D. M. Mittleman, C. Rich, V. L. Colvin, *Phys. Rev. E* **2005**, *71*, 016615.
[24] E. Palacios-Lidon, B. H. Juárez, E. Castillo-Martínez, C. López, *J. Appl. Phys.* **2005**, *97*, 063502.
[25] S. G. Romanov, S. Orlov, A. V. Korovin, O. Zhuromskyy, N. Vogel, K. Landfester, C. K. Weiss, U. Peschel, in *Interplay of Mie and Bragg resonances in partly ordered monolayers of colloidal spheres* (Eds: H. R. Míguez, S. G. Romanov, L. C. Andreani, C. Seassal), **2012**, p. 84250V https://doi.org/10.1117/12.923433.
[26] A. N. Poddubny, M. V. Rybin, M. F. Limonov, Y. S. Kivshar, *Nat. Commun.* **2012**, *3*, 914.
[27] M. A. Kaliteevski, J. Manzanares Martinez, D. Cassagne, J. P. Albert, *Phys. Status Solidi A* **2003**, *195*, 612.
[28] L. A. Dorado, R. A. Depine, G. Lozano, H. Míguez, *Phys. Rev. B* **2007**, *76*, 245103.
[29] J. A. Pariente, N. Caselli, C. Pecharromán, Á. Blanco, C. López, *Small* **2020**, *16*, 2002735.
[30] P. D. García, R. Sapienza, Á. Blanco, C. López, *Adv. Mater.* **2007**, *19*, 2597.
[31] J. F. Galisteo-López, E. Palacios-Lidón, E. Castillo-Martínez, C. López, *Phys. Rev. B* **2003**, *68*, 115109.
[32] P. D. García, R. Sapienza, L. S. Froufe-Pérez, C. López, *Phys. Rev. B* **2009**, *79*, 241109.
[33] V. N. Astratov, A. M. Adawi, S. Fricker, M. S. Skolnick, D. M. Whittaker, P. N. Pusey, *Phys. Rev. B* **2002**, *66*, 165215.

 

[34] J. F. Galisteo-López, M. Ibisate, R. Sapienza, L. S. Froufe-Pérez, Á. Blanco, C. López, *Adv. Mater.* **2011**, *23*, 30.
[35] M. Galli, S. L. Portalupi, M. Belotti, L. C. Andreani, L. O'Faolain, T. F. Krauss, *Appl. Phys. Lett.* **2009**, *94*, 071101.
[36] J. F. Galisteo-López, F. García-Santamaría, D. Golmayo, B. H. Juárez, C. López, E. Palacios-Lidon, *J. Opt. A: Pure Appl. Opt.* **2005**, *7*, S244.
[37] Z. Zhang, S. Satpathy, *Phys. Rev. Lett.* **1990**, *65*, 2650.
[38] P. Van Rysselberghe, *J. Phys. Chem.* **1932**, *36*, 1152.
[39] D. A. G. Bruggeman, *Ann. Phys.* **1937**, *421*, 160.
[40] O. Painter, R. K. K. Lee, A. Scherer, A. Yariv, J. D. O'Brien, P. D. Dapkus, I. Kim, *Science* **1999**, *284*, 1819.
[41] T. W. Ebbesen, H. J. Lezec, H. F. Ghaemi, T. Thio, P. A. Wolff, *Nature* **1998**, *391*, 667.